Forward Kinematics and Control of a Segmented Tunable-Stiffness 3-D Continuum Manipulator

Shivangi Misra and Cynthia Sung

***Abstract*— In this work, we consider the problem of controlling the end effector position of a continuum manipulator through local stiffness changes. Continuum manipulators offer the advantage of continuous deformation along their lengths, and recent advances in smart material actuators further enable local compliance changes, which can affect the manipulator's bulk motion. However, leveraging local stiffness change to control motion remains lightly explored. We build a kinematic model of a continuum manipulator as a sequence of segments consisting of symmetrically arranged springs around the perimeter of every segment, and we show that this system has a closed form solution to its forward kinematics. The model includes common constraints such as restriction of torsional or shearing movement. Based on this model, we propose a controller on the spring stiffnesses for a single segment and provide provable guarantees on convergence to a desired goal position. The results are verified in simulation and compared to physical hardware.**

I. Introduction

Soft robots have a plethora of advantages compared to traditional rigid robots [1], including the ability to deform continuously, adapt to unknown situations, demonstrate compliance matching, and perform force feedback through embodied sensing in many applications [2], [3], [4]. Latticed or tessellated structures provide programmable compliance in the robot body, with a large range of achievable stiffnesses [5], [6]. However, most soft robots designed from these structures use global actuation strategies such as air pressure [7], vacuum [8], or tendons [9]. Consequently, they do not take advantage of opportunities for stiffness tuning along the body of the robot.

Giving soft robots the ability to locally tune their bodily stiffness may enable them to operate more efficiently in changing external conditions. Animals often tune their body stiffnesses to improve stability and agility of their movements in this way [10], [11]. This behavior is achieved through a combination of large global and smaller local muscles in the body, with global muscles controlling bulk movement and local muscles generally adjusting local stiffness [12]. Recent advancements in smart materials and actuators have produced electrically [13], thermally [14], [15], and magnetically [16] responsive materials that can be embedded directly and controlled locally within a robot body for similar actuation strategies. These platforms for distributed actuation promise future robots with the ability to alter local rigidity and forces independently from position [17].

However, modeling and controlling such tunable stiffness systems remains challenging due to the complexity of the forward kinematics and control problem. Modeling soft continuum manipulators typically involves a series of mappings: transforming variables from actuation space to configuration space, and thereafter to the robot's task space [18], [1], [19]. The second mapping is robot-independent and proposed transformations from previous studies are equivalent [18]. It is the former half of the mapping scheme which is robot-specific and challenging. Common approaches include Bernoulli-Euler beam mechanics [20], Cosserat-rod theory [21], pseudo-rigid models [22], or iterative FEA models [23]. Beam models are generalizable across different compliant structures though limiting due to small deflection assumptions and suffer from inaccuracies due to numerical approximations [24], [25]. While FEA based methods may be more accurate, they are known to be computationally expensive [26]. Other existing methods are restricted in applicability to robots with global actuation schemes with single or binary compliance modes [27], [28] or those that exhibit solely planar deformation using antagonistic actuators [29], [30]. The problem of modeling and control of local distributed regions of the manipulator substrate thus still remains largely unexplored.

We aim to tackle the problem of tunable stiffness control in a 3D compliant manipulator arm, paving the way for future soft robotic applications that take advantage of the potential brought by smart materials and distributed actuation. In order to gain insights into this problem, we consider the relatively simple case of a segmented 3D arm with tunable stiffness elements distributed throughout its outer skin and a single tendon down the center. In the context of this problem, we propose a model for the manipulator arm and show that there exists an analytical solution for the arm's configuration under quasistatic assumptions. Building on this intuition, we then construct a controller that enables the manipulator to stabilize at a desired end effector position through tuning of stiffnesses alone. The contributions of this paper include:

- a new theoretical model for 3D compliant manipulators with a tunable stiffness material skin;
- an analytical solution to the forward kinematics problem applied to this model;
- analytical gradients (how changes in stiffness affect end effector position); and
- a stiffness-based controller for moving the end effector

Support for this project has been provided in part by NSF Grant No. 1845339 and by the Army Research Office (ARO) under MURI award #W911NF1810327. The authors also thank Yifan Yuan and Jeremy Wang for fabrication assistance, and Wei-Hsi Chen, Dr. Dan Koditschek, and Dr. Victor Preciado for helpful discussions.

S. Misra and C. Sung are with the General Robotics, Automation, Sensing & Perception (GRASP) Lab at the University of Pennsylvania, Philadelphia, PA, USA. {shivangi, crsung}@seas.upenn.edu

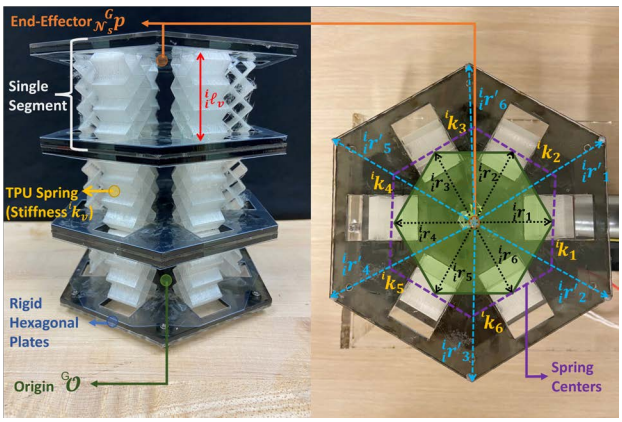

Fig. 1. Side and top view of continuum manipulator prototype

to a desired position with stability and convergence guarantees.

The model and algorithms are verified in simulation and through experimental results.

The remainder of this paper is structured as follows. Section II describes our manipulator model and the problem to be solved. Section III explains the forward kinematics for this manipulator. Section IV details our approach to position control for a single segment and proof of stability. Section V includes a experimental validation of our forward kinematics algorithm for both single and multi-segment arms. We also present the results of stiffness controller tests in simulation. Section VI concludes with a discussion of the results and directions for future work.

II. Model Definition and Problem Statement

Consider the soft continuum manipulator in Fig. 1. The manipulator is composed of N_s segments $i \in \{1, \ldots, N_s\}$. Each segment consists of a top plate and a bottom plate connected via N_v springs with a natural length ℓ_0 and located at a distance R from the center. We call R the radius of the manipulator. In their natural uncompressed state, all of the segments look identical and are rotationally symmetric. The segments are connected end-to-end such that the top of segment i is connected to the bottom of segment $i+1$.

The pictured manipulator can be actuated via two means. A single tendon runs down the center of the manipulator, providing a length constraint that controls the overall manipulator deformation similarly to current global actuation schemes. In addition, this theoretical manipulator is made of tunable stiffness materials, which have the affect of locally changing the stiffness of the springs around the circumference of the arm. When the tendon is pulled, the entire manipulator contracts in length into a final global configuration that depends on the stiffness distribution in the $N_s \times N_v$ springs. It is thus possible to control the end effector position simply via local stiffness tuning.

A. Single Segment Model

For a single segment i, we define a local reference frame ${}^{i}\mathcal{O}$, with an origin at the center of the bottom plate of the segment and the ${}^{i}\mathbf{z}$ axis oriented normal to the plate. The position of the center of the top plate of segment i in the frame of segment j is written as ${}^{j}_{i}\mathbf{p} = \left[{}^{j}_{i}x, {}^{j}_{i}y, {}^{j}_{i}z\right]^{\mathsf{T}}$. The orientation of the top plate is written as a quaternion ${}^{j}_{i}\mathbf{q} = \left[{}^{j}_{i}q_w, {}^{j}_{i}q_x, {}^{j}_{i}q_y, {}^{j}_{i}q_z\right]^{\mathsf{T}}$. These two quantities combined describe the full state of the segment

$$ {}^{j}_{i}\mathcal{S} = \left[{}^{j}_{i}\mathbf{p},\ {}^{j}_{i}\mathbf{q}\right]^{\mathsf{T}} \tag{1} $$

Note that ${}^{j}_{i}\mathcal{S}$ also describes the origin and orientation of frame ${}^{i+1}\mathcal{O}$ as written in frame ${}^{j}\mathcal{O}$. The global frame is ${}^{G}\mathcal{O}$.

Each segment contains N_v springs located at even intervals around its circumference. Let ${}^{i}k_v$, $v \in \{1, \ldots, N_v\}$, be the stiffness of the vth spring in the ith segment, and let ${}^{j}_{i}\boldsymbol{\ell}_v$ be the vector along the length of the spring. We use the variable ${}^{i}\mathcal{K}$ to denote the vector of stiffness values $[{}^{i}k_1, \ldots, {}^{i}k_{N_v}]$. Let ${}^{j}_{i}\mathbf{r}_v = R\left[\cos\theta_v, \sin\theta_v, 0\right]^{\mathsf{T}}$, where $\theta_v = \frac{2\pi v}{N_v}$, be the radial vector defining the location of the bottom of spring v relative to ${}^{i}\mathcal{O}$ as written in ${}^{j}\mathcal{O}$. Then the pose of spring v is related to the state of the segment as

$$ {}^{j}_{i}\boldsymbol{\ell}_v = {}^{j}_{i}\mathbf{p} + \left(\mathbf{Rot}\left({}^{j}_{i}\mathbf{q}\right){}^{j}_{i}\mathbf{r}_v - {}^{j}_{i}\mathbf{r}_v\right) \tag{2} $$

where $\mathbf{Rot}\left(\mathbf{q}\right)$ is the 3-D rotation matrix corresponding to the quaternion $\mathbf{q}$.

a) Kinematic Constraints: In many cases [9], [18], a soft manipulator is subject to symmetry and length constraints (ref. Fig. 2). In particular, a tubular continuum manipulator with a continuous skin will often exhibit:

1) No torsion: The outer skin will constrain each segment so that there is no torsion about the center axis of the segment. Mathematically, this translates to a kinematic constraint that orientation ${}^{i}_{i}\mathbf{q}$ will never have a ${}^{i}\mathbf{z}$-component, i.e., that ${}^{i}_{i}q_z = 0$.
2) No shear: The outer skin will constrain each segment to minimize shear. This means that all of the springs ${}^{i}_{i}\boldsymbol{\ell}_v$ will remain parallel to each other and to the vector ${}^{i}_{i}\mathbf{p}$ between the centers of the top and bottom plates. As in Fig. 2, only one solution for the orientation is stable at the inclination ${}^{i}\alpha$ and extension ${}^{i}d$ among the loci of solutions indicated. Following the relations between key angles in a trapezoid shape such as the one indicated in the Fig. 2, one can easily deduce that this implies that the angle of inclination of the segment will be half the angle of rotation of the top platform.

Finally, by observing that a segment cannot self-intersect and therefore the extreme orientation of a segment produces an isosceles triangle, we can also obtain an upper bound on the maximum allowable inclination to prevent ground or self-collision as

$$ \cos^{-1}\left(\frac{{}^{i}_{i}z}{{}^{i}d}\right) \leq \sin^{-1}\left(\frac{{}^{i}d}{2R_o}\right) \tag{3} $$

where R_o is the outer radius of the manipulator plates (which may not be the same as the radius at which the springs act) and

$$ {}^{i}d = \|{}_{i}\mathbf{p}\| = \sqrt{{}^{i}_{i}x^2 + {}^{i}_{i}y^2 + {}^{i}_{i}z^2} \tag{4} $$

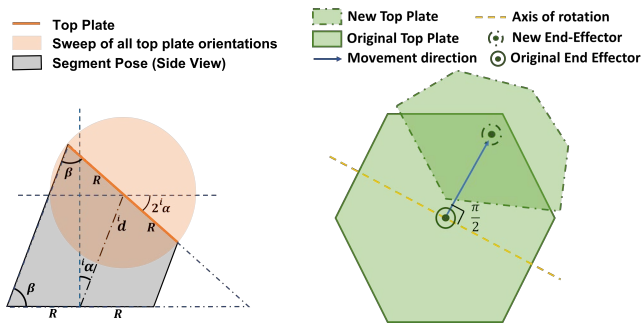

Fig. 2. The vertical cross-section through the end-effector of a manipulator segment is an isosceles trapezoid. It follows that angle of inclination is ${}^i\alpha$ while angle of rotation is $2\,{}^i\alpha$; the second image shows the segment's projection onto the X-Y plane, ${}^i\gamma$ is the radial direction in which the segment tilts and that the axis of rotation passing through the end-effector is always perpendicular to the radial direction of tilt.

is the "length" of segment i.

B. Multi-Segment Manipulator Model

The multi-segment manipulator consists of multiple symmetrically stacked segments. We calculate the position of the end effector by composing the transformation matrices $\mathbf{T}\left({}^i_i\mathcal{S}\right)$ corresponding to each segment

$$\begin{pmatrix} {}^G_{N_s}\mathbf{p} \\ 1 \end{pmatrix} = \mathbf{T}\left({}^{N_s}_{N_s}\mathcal{S}\right) \times \mathbf{T}\left({}^{N_s-1}_{N_s-1}\mathcal{S}\right) \cdots \times \mathbf{T}\left({}^1_1\mathcal{S}\right) \begin{pmatrix} \hat{\mathbf{z}} \\ 1 \end{pmatrix} \quad (5)$$

a) Kinematic Constraints: The tendon down the center of the manipulator passes through the center of the top and bottom plates of each segment. As a result, the manipulator's state must also satisfy that

$$\sum_{i=1}^{N_s} \|{}_i\mathbf{p}\| = \ell_t \quad (6)$$

C. Problem Statement

We formally define the problems addressed in this paper.

Problem 2.1 (Forward Kinematics): Given an N_s-segment manipulator with spring stiffnesses ${}^ik_v$ and tendon length ℓ_t, find the position ${}^G_{N_s}\mathbf{p}$ and orientation ${}^G_{N_s}\mathbf{q}$ of the end effector.

Problem 2.2 (Single Segment Stiffness Control): Given an N_s-segment manipulator and a desired global position $\mathbf{p}^{des}$ for the end effector, find the stiffness values ${}^ik_v$ for each spring and the tendon length ℓ_t such that the error in the position of the end effector ${}^G_{N_s}\mathbf{p} - \mathbf{p}^{des}$ is less than an error threshold ϵ.

III. Forward Kinematics

To solve the forward kinematics problem, we analyze the potential energy of the spring system. For a given configuration, the potential energy stored in the manipulator can be written as

$$E = \frac{1}{2}\sum_{i=1}^{N_s}\sum_{v=1}^{N_v} {}^ik_v \left(\ell_0 - \|{}^i_i\boldsymbol{\ell}_v\|_2\right)^2 \quad (7)$$

At any point in time, the system tends to the state of lowest energy, that is, to the solution of the optimization problem

$$\min_{{}^G_i\mathcal{S}} E \quad (8)$$

subject to the kinematic constraints of the manipulator.

A. Single Segment Forward Kinematics

We first show that a single segment has 3 degrees of freedom. Consider the segment i. Let the axis of rotation of the top plate be ${}^i_i\mathbf{a} = \left[{}^i_ia_x, {}^i_ia_y, {}^i_ia_z\right]^\intercal$ and ${}^i\alpha$ be the angle of rotation of the top plate about ${}^i_i\mathbf{a}$. Due to the kinematic constraints listed in Section II-A, we know that the following relations hold:

$${}^i_i\mathbf{a} = \frac{1}{\sqrt{{}^i_ix^2 + {}^i_iy^2}}\left[-{}^i_iy, \quad {}^i_ix, \quad 0\right] \quad (9)$$

$${}^i\alpha = \tan^{-1}\left[\frac{\sqrt{{}^i_ix^2 + {}^i_iy^2}}{{}^i_iz}\right]. \quad (10)$$

Then the orientation of the segment reduces to

$${}^i_i\mathbf{q} = \left[\cos{}^i\alpha, {}^i_ia_x\sin{}^i\alpha, {}^i_ia_y\sin{}^i\alpha, {}^i_ia_z\sin{}^i\alpha\right]^\intercal \quad (11)$$

Substituting into our representation of the segment's state, we obtain

$${}^i_i\mathcal{S} = \left[{}^i_ix, {}^i_iy, {}^i_iz, \frac{{}^i_iz}{{}^id}, \frac{-{}^i_iy}{{}^id}, \frac{{}^i_ix}{{}^id}, 0\right]^\intercal \quad (12)$$

Now, we can use this reduced state to compute the forward kinematics. By substituting Eq. (2) and (12) into Eq. (7), we obtain the segment's energy ${}^iE$:

$${}^iE = \frac{1}{2}\sum_{v=1}^{N_v} {}^ik_v\left(\ell_0 - {}^id + \frac{2R}{{}^id}\left({}^i_ix\cos\theta_v + {}^i_iy\sin\theta_v\right)\right)^2 \quad (13)$$

The use of the implicit tendon constraint (single segment) essentially reduces the search space of the problem to a two dimensional plane (see Appendix for derivation). Let ${}^i_i\xi = [{}^i_ix, {}^i_iy]^\intercal$. The equilibrium pose of the segment can thus be found by solving for ${}^i_i\xi$ at which $\frac{\partial\,{}^iE}{\partial\,{}^i_ix} = \frac{\partial\,{}^iE}{\partial\,{}^i_iy} = 0$:

$$\begin{pmatrix} {}^i_ix & {}^i_iy \end{pmatrix}^\intercal = \left({}^i\mathbf{A}\right)^{-1}\left(-{}^i\mathbf{B}\right) \quad (14)$$

where

$${}^i\mathbf{A} = \begin{pmatrix} \sum_{v=1}^{N_v} {}^ik_v\cos^2\theta_v & \sum_{v=1}^{N_v} {}^ik_v\cos\theta_v\sin\theta_v \\ \sum_{v=1}^{N_v} {}^ik_v\cos\theta_v\sin\theta_v & \sum_{v=1}^{N_v} {}^ik_v\sin^2\theta_v \end{pmatrix}, \quad (15)$$

$${}^i\mathbf{B} = \frac{{}^id(\ell_0 - {}^id)}{2R}\begin{pmatrix} \sum_{v=1}^{N_v} {}^ik_v\cos\theta_v \\ \sum_{v=1}^{N_v} {}^ik_v\sin\theta_v \end{pmatrix}. \quad (16)$$

Notice that ${}^i\mathbf{A}$ is always non-singular unless ${}^ik_v = 0$ for all v. The value of ${}^i_iz$ can be recovered from the tendon constraint in Eq. (4).

This analytical solution does not account for the collision constraints in Eq. (3). Practically, when solving the system of equations, the exact solution including collision constraints can be determined by projecting the solution to Eq. (14) onto the closest point on the workspace boundary defined by Eq. (3) such that the segment length remains equal to ${}^id$.

B. Multi-Segment Forward Kinematics

To extend these results to a multi-segment manipulator, we observe that the tendon down the center of the manipulator acts solely as a length constraint and does not impact the bending of any of the segments. Thus, the full forward kinematics problem can be decoupled into two separate problems: 1) what is the length of each of the segments? and 2) what is the bending angle of each of the segments? Note that the second problem is exactly the one solved in Section III-A. It thus only remains to determine the length of each of the segments.

Because the segments are separated from each other via rigid plates, each of the segments can be replaced by an equivalent spring matching the bulk linear and bending stiffness of the N_v original springs. Thus, the entire manipulator can be treated as springs in series subject to a total length constraint. The equivalent linear stiffness for a single segment is

$$ {}^{i}K_{eq} = \sum_{v=1}^{N_v} {}^{i}k_v \tag{17} $$

so the length of each segment is computed as

$$ {}^{i}d = \ell_0 - \left(\frac{(N_s \ell_0 - \ell_t)}{{}^{i}K_{eq}} \left(\sum_{j=1}^{N_s} \frac{1}{{}^{j}K_{eq}} \right)^{-1} \right) \tag{18} $$

IV. Single Segment Stiffness Control

This manipulator can be controlled to stabilize to a desired end effector position $\mathbf{p}^{des}$ by changing the stiffness distribution. The energy landscape in 3-D Euclidean space morphs as stiffness values around the segment change, and the segment i tends to the state of lowest energy at all times. Controlling the manipulator configuration is thus a matter of moving the energy minimum to the desired end effector position along a continuous trajectory. We set the tendon length to match the distance to desired position, $\ell_t = \|\mathbf{p}^{des}\|$ and in doing so, constrain the movement of the end-effector to a spherical surface.

The intuition behind our proposed controller is as follows: From the kinematic analysis, we know that $\frac{d\,{}^{i}E}{d\,{}^{i}_{i}\xi} = {}^{i}\mathbf{A}\,{}^{i}_{i}\xi + {}^{i}\mathbf{B}$. Then, for any given energy landscape, the top plate of segment i will move in the direction of $-\frac{d\,{}^{i}E}{d\,{}^{i}_{i}\xi}$. Thus, we define

$$ {}^{i}\mathbf{M} = \frac{\partial\,{}^{i}\mathbf{A}}{\partial\,{}^{i}\mathcal{K}}\,{}^{i}_{i}\xi + \frac{\partial\,{}^{i}\mathbf{B}}{\partial\,{}^{i}\mathcal{K}} \tag{19} $$

(In a slight abuse of notation, we use $\frac{\partial\,{}^{i}\mathbf{A}}{\partial\,{}^{i}\mathcal{K}}$ to represent for each value ${}^{i}k_v \in {}^{i}\mathcal{K}$, the matrix corresponding to $\frac{\partial\,{}^{i}\mathbf{A}}{\partial\,{}^{i}k_v}$ such that $\frac{\partial\,{}^{i}\mathbf{A}\,{}^{i}_{i}\xi}{\partial\,{}^{i}\mathcal{K}} = \frac{\partial\,{}^{i}\mathbf{A}}{\partial\,{}^{i}\mathcal{K}}\,{}^{i}_{i}\xi = [\frac{\partial\,{}^{i}\mathbf{A}}{\partial\,{}^{i}k_1}, \frac{\partial\,{}^{i}\mathbf{A}}{\partial\,{}^{i}k_2}, \cdots \frac{\partial\,{}^{i}\mathbf{A}}{\partial\,{}^{i}k_{N_v}}]\,{}^{i}_{i}\xi$ assuming ${}^{i}_{i}\xi$ is constant with respect to ${}^{i}\mathcal{K}$.) This expression is equivalent to the partial derivative of the gradient of the energy function with respect to stiffnesses ${}^{i}\mathcal{K}$ when the end effector position is not constrained to be at the point of lowest energy. For a given change in stiffness values ${}^{i}\dot{\mathcal{K}}$, we then expect the segment end-effector to move in a direction whose projection onto the X-Y plane will be $-({}^{i}\mathbf{M}\,{}^{i}\dot{\mathcal{K}})$. The problem is then to find the ${}^{i}\dot{\mathcal{K}}$ such that this product aligns most closely with $(\xi^{des} - {}^{i}_{i}\xi)$.

In general, the solution to this problem will be to use

$$ {}^{i}\dot{\mathcal{K}} = -{}^{i}\mathbf{M}^{\dagger}\left(\xi^{des} - {}^{i}_{i}\xi\right) \tag{20} $$

Practically, since the physical system will also be subject to lower and upper bounds on ${}^{i}\mathcal{K}$, we solve the constrained optimization problem

$$ \min_{{}^{i}\dot{\mathcal{K}}} \left({}^{i}\mathbf{M}\,{}^{i}\dot{\mathcal{K}}\right) \cdot (\xi^{des} - {}^{i}_{i}\xi) \tag{21} $$

A. Convergence and Stability

It can be shown that this single segment stiffness controller always stably converges to the desired end effector position, provided it is within the reachable workspace. Note that throughout this paper, we assume quasi-static behavior. When the stiffness changes $\|{}^{i}\mathcal{K}\|$ are low and the damping is high, the system can be treated as a continuous system that follows the path in Eq. (14) exactly.

Lemma 4.1: Assuming stiffness and workspace bounds are not reached, a single segment using the controller in Eq. (21) will always converge to the desired position $\mathbf{p}^{des}$.

Proof: Consider the following Lyapunov function

$$ V({}^{i}_{i}\xi) = \left({}^{i}_{i}\xi - \xi^{des}\right)^2 \tag{22} $$

which exists over all possible ${}^{i}_{i}\xi$. It is clear that $V \geq 0$ for all ${}^{i}_{i}\xi$ and $V = 0$ only when ${}^{i}_{i}\xi = \xi^{des}$. Further, as shown previously, ${}^{i}_{i}\xi = \xi^{des}$ only when ${}^{i}_{i}\mathbf{p} = \mathbf{p}^{des}$.

Then the time derivative of this function is

$$ \dot{V} = 2\left({}^{i}_{i}\xi - \xi^{des}\right) \cdot \frac{d\,{}^{i}_{i}\xi}{dt} \tag{23} $$

which can be expanded as

$$ \dot{V} = 2\left({}^{i}_{i}\xi - \xi^{des}\right) \cdot \frac{d\,{}^{i}_{i}\xi}{d\,{}^{i}\mathcal{K}}\,{}^{i}\dot{\mathcal{K}} \tag{24} $$

Based on our FK model, for given tendon length ℓ_t and set of stiffnesses ${}^{i}\mathcal{K}$, the segment follows a trajectory defined by ${}^{i}\mathbf{A}\,{}^{i}_{i}\xi + {}^{i}\mathbf{B} = 0$. Taking the derivative of both sides with respect to ${}^{i}\mathcal{K}$ yields

$$ \frac{\partial\,{}^{i}\mathbf{A}}{\partial\,{}^{i}\mathcal{K}}\,{}^{i}_{i}\xi + {}^{i}\mathbf{A}\frac{\partial\,{}^{i}_{i}\xi}{\partial\,{}^{i}\mathcal{K}} + \frac{\partial\,{}^{i}\mathbf{B}}{\partial\,{}^{i}\mathcal{K}} = 0 \tag{25} $$

$$ {}^{i}\mathbf{A}^{-1}\left(-\frac{\partial\,{}^{i}\mathbf{B}}{\partial\,{}^{i}\mathcal{K}} - \frac{\partial\,{}^{i}\mathbf{A}}{\partial\,{}^{i}\mathcal{K}}\,{}^{i}_{i}\xi\right) = \frac{\partial\,{}^{i}_{i}\xi}{\partial\,{}^{i}\mathcal{K}} \tag{26} $$

At the same time, our stiffness controller Eq. (20) is to use

$$ {}^{i}\mathbf{M}\,{}^{i}\dot{\mathcal{K}} = \left(\frac{\partial\,{}^{i}\mathbf{A}}{\partial\,{}^{i}\mathcal{K}}\,{}^{i}_{i}\xi + \frac{\partial\,{}^{i}\mathbf{B}}{\partial\,{}^{i}\mathcal{K}}\right)\,{}^{i}\dot{\mathcal{K}} = {}^{i}_{i}\xi - \xi^{des} \tag{27} $$

when stiffness bounds are not reached. We note that ${}^{i}\mathbf{M}$ has full row rank and therefore, its right pseudo-inverse always

exists implying that there will always be at least one value for ${}^{i}\dot{\mathcal{K}}$ that exactly solves this equation.

Finally, substituting Eq. (26) and (27) into Eq. (24), we find that

$$\dot{V} = 2\left({}^{i}_{i}\xi - \xi^{des}\right) \cdot \left[{}^{i}\mathbf{A}^{-1}\left(-\frac{\partial\, {}^{i}\mathbf{B}}{\partial\, {}^{i}\mathcal{K}} - \frac{\partial\, {}^{i}\mathbf{A}}{\partial\, {}^{i}\mathcal{K}}\, {}^{i}_{i}\xi\right)\right] {}^{i}\dot{\mathcal{K}} \quad (28)$$

$$= -2\left({}^{i}_{i}\xi - \xi^{des}\right)^{\intercal} {}^{i}\mathbf{A}^{-1}\left({}^{i}_{i}\xi - \xi^{des}\right) \quad (29)$$

Since the matrix ${}^{i}\mathbf{A}$ can be decomposed as,

$${}^{i}\mathbf{A} = \frac{2R}{{}^{i}d} C\Lambda C^{\intercal} \quad (30)$$

where,

$$C = \begin{pmatrix} \cos\theta_1 \cdots \cos\theta_{N_v} \\ \sin\theta_1 \cdots \sin\theta_{N_v} \end{pmatrix}, \Lambda = \begin{pmatrix} {}^{i}k_1 & \cdots & 0 \\ \vdots & \ddots & \vdots \\ 0 & \cdots & {}^{i}k_{N_v} \end{pmatrix}$$

and since ${}^{i}\mathbf{A} = \frac{2R}{{}^{i}d} C\Lambda C^{\intercal} = \frac{2R}{{}^{i}d}(C\Lambda^{1/2})(C\Lambda^{1/2})^{\intercal}$, ${}^{i}\mathbf{A}$ is positive definite and the controller is Lyapunov. ■

This proof applies whenever the stiffness bounds are not reached. Even if this constraint is not satisfied, it is clear that a solution such that

$$\left(\frac{\partial\, {}^{i}\mathbf{A}}{\partial\, {}^{i}\mathcal{K}}\, {}^{i}_{i}\xi + \frac{\partial\, {}^{i}\mathbf{B}}{\partial\, {}^{i}\mathcal{K}}\right) {}^{i}\dot{\mathcal{K}} \cdot \left({}^{i}_{i}\xi - \xi^{des}\right) \leq 0 \quad (31)$$

always exists, and thus the system is marginally stable in the sense of Lyapunov.

V. Results

We tested our kinematic analysis and stiffness controller in simulation and verified the kinematic analysis on a hardware platform. In all cases, $N_v = 6$. For simulations, we used MATLAB on an Intel i5-8300H processor with 16GB installed RAM. To solve the optimization problem in Eq. (21), we use the `lsqlin` solver with the interior-point algorithm.

A. Forward Kinematics

To verify the model and forward kinematics equations, we constructed a soft manipulator using TPU springs [31] separated by rigid acrylic plates of weight 58g approximately. The springs are diamond-lattice shaped springs of dimensions 30 × 23 × 20.2 (mm), weighing 3g on average. They are positioned on separating plates as in Fig. 1 with $R = 25$ mm and $R_o = 63$ mm. A motor-pulley mechanism controls the length of a central nylon tendon passing through the middle of each rigid plate. Using this setup, we tested various stiffness distributions and measured the end effector positions in an OptiTrack motion capture system and compared the results to the model.

Figure 3a shows the results for a single segment manipulator model with lower stiffnesses in the $-x$ direction. The segment was contracted from an initial tendon length of 31 mm to a final length of 11 mm. A slice of the energy landscape which contains the solution trajectories is shown in Fig. 3b. Note that the energy landscape is convex, and the end-effector trajectory passes through regions of lowest energy for each tendon length. Figure 3c shows a comparison of the final pose and trajectory generated by the FK model and that from the physical manipulator. The RMSE error in trajectories is 0.7705 mm. We attribute this marginal error to non-linearity in the TPU springs' physical properties.

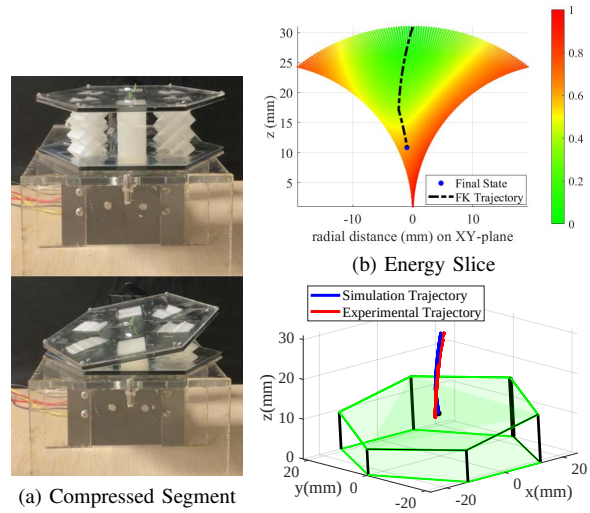

(a) Compressed Segment (b) Energy Slice (c) Single Segment: Simulation

Fig. 3. Segment with ${}^{i}\mathcal{K} = \{1.93, 0.83, 0.62, 0.50, 0.60, 0.60\}$. (a) Initial and final pose when tendon is contracted. (b) Slice of energy landscape with trajectory of end effector overlaid. (c) Simulated vs. experimental trajectory.

TABLE I

3-Segment Manipulator Stiffness Values

Segment	Configuration I (N/mm)	Configuration II (N/mm)
1	[1.57, 1.59, 1.63, 1.58, 1.60, 1.52]	[1.62, 1.60, 1.60, 0.58, 0.52, 0.52]
2	[1.41, 1.51, 2.09, 2.35, 2.19, 1.42]	[2.08, 1.83, 2.35, 1.94, 2.19, 1.86]
3	[1.27, 1.37, 1.83, 1.95, 1.86, 1.41]	[1.02, 1.37, 1.41, 1.42, 1.41, 1.27]

Results for a multi-segment manipulator are shown in Fig. 4. We constructed a 3 segment manipulator (segments numbered from bottom to top) with two different stiffness configurations, shown in Table I. In this case, the tendon was pulled down from the manipulator's relaxed height of 93 mm to a length of 33 mm in configuration (1) and to 28 mm in configuration (2). The trajectories of the physical manipulator and its simulated model match in form with an RMSE error of 1.1942 mm in configuration (1) and 2.2918 mm in configuration (2).

B. Single Segment Control

The stiffness controller is theoretically proven to converge. We add further empirical evidence by running 40 trials on a single segment manipulator of radius 8 mm and rest height 10 mm with randomly initialized stiffness distributions and goal positions within its valid workspace. In all cases, the segment successfully converges to the desired goal position, ending with a different final stiffness distribution. Mean convergence times (defined as error<0.05 mm) for the trials was 91 s with a standard deviation of 44.5 s. Control actions in each iteration are computed in less than 60ms.

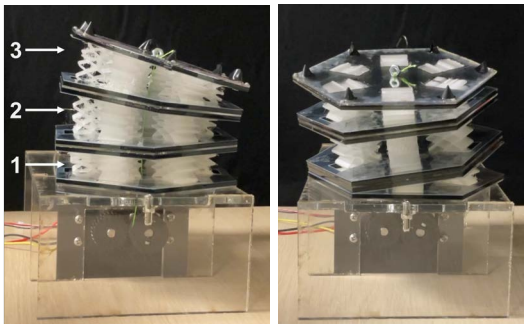

(a) Configuration I (b) Configuration II

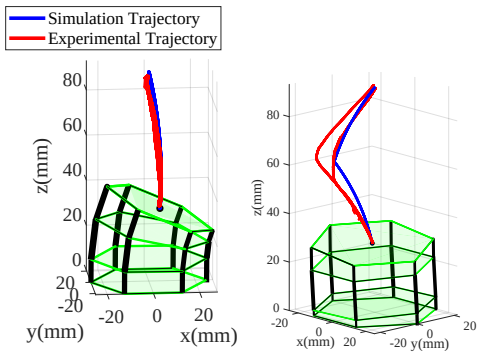

(c) FK for Configuration I (d) FK for Configuration II

Fig. 4. Manipulator with two stiffness configurations as in Table I. (a) Pose in Configuration I. (b) Pose in Configuration II. (c) Simulated vs. experimental trajectory in Configuration I. (d) Simulated vs. experimental trajectory in Configuration II.

We also ran a set of 20 tests where the segment starts with randomized initial stiffnesses and aims to reach the same goal position $[0.9, 0.3, 4.5]^\intercal$. The stiffness controller was successful in all cases. Figure 5 shows the evolution of stiffness values of two segments that were initialized with different stiffness distributions, but had identical trajectories. We observe from Fig. 5a and 5b that the ending stiffness distribution also looks similar. Interestingly, in case 1, we see all stiffnesses converge to their average before redistributing to reach their final values.

VI. Discussion

In this work, we present a model for a theoretical segmented continuum manipulator with locally variable stiffnesses. We derive a closed form expression for the forward kinematics of a manipulator with multiple segments. The validity of this method is shown in simulation by ensuring that the end-effector always follows a path of lowest energy and comparing the movement of the simulated manipulator with that of a physical prototype. Additionally, we proposed a controller for a single segment which manipulates local stiffnesses to achieve a desired pose. We show stability is guaranteed with this controller and verify this experimentally.

An advantage of the proposed methods is in its applicability to a large set of soft manipulators and potential future applications that benefit from stiffness control. Future work involves adapting our current algorithms for non-linear springs, as well as extending the single segment stiffness

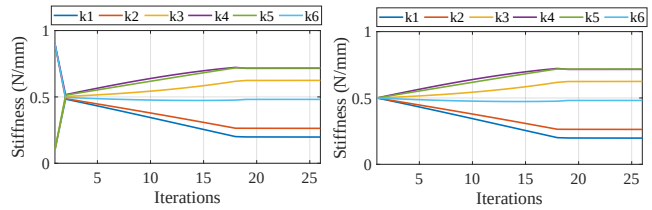

(a) Stiffness Change: Case 1 (b) Stiffness Change: Case 2

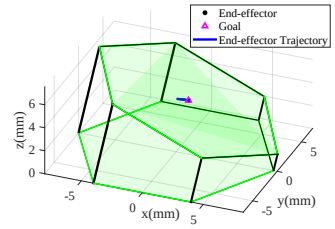

Fig. 5. Simulation results for stiffness control of a single segment with desired goal $[0.9, 0.3, 4.5]^\intercal$. (a) Segment initialized with ${}^i\mathcal{K} = \{0.9, 0.1, 0.9, 0.1, 0.9, 0.1\}$ N/mm. (b) Segment initialized with ${}^i\mathcal{K} = \{0.5, 0.5, 0.5, 0.5, 0.5, 0.5\}$ N/mm.

controller to manipulators with multiple segments. We also plan to validate our stiffness control on a physical setup where local stiffnesses are varied in real-time. For such a system, it would be preferred if the variation in stiffness around the segment is minimized (thus distributing stress more evenly throughout the segment).

Appendix

A. Derivation of Energy with Implicit Constraints (Eq. (13))

First, the rotation matrix in Eq. (12) is,

$$\mathbf{Rot}\left({}^i_i\mathbf{q}\right) = \frac{1}{{}^id^2}\begin{bmatrix} -{}^i_ix^2 + {}^i_iy^2 + {}^i_iz^2 & -2{}^i_ix{}^i_iy & 2{}^i_ix{}^i_iz \\ -2{}^i_ix{}^i_iy & {}^i_ix^2 - {}^i_iy^2 + {}^i_iz^2 & 2{}^i_iy{}^i_iz \\ -2{}^i_ix{}^i_iz & -2{}^i_iy{}^i_iz & -{}^i_ix^2 - {}^i_iy^2 + {}^i_iz^2 \end{bmatrix} \tag{32}$$

Substituting the constraint Eq. (6) reveals

$$= \frac{1}{{}^id^2}\begin{bmatrix} {}^id^2 - 2\,{}^i_ix^2 & -2\,{}^i_ix\,{}^i_iy & 2\,{}^i_ix\,{}^i_iz \\ -2\,{}^i_ix\,{}^i_iy & {}^id^2 - 2\,{}^i_iy^2 & 2\,{}^i_iy\,{}^i_iz \\ -2\,{}^i_ix\,{}^i_iz & -2\,{}^i_iy\,{}^i_iz & {}^id^2 - 2\,{}^i_ix^2 - 2\,{}^i_iy^2 \end{bmatrix} \tag{33}$$

Substituting into Eq. (2) yields

$${}^i_i\boldsymbol{\ell}_v = \frac{1}{{}^id^2}\,{}^i_i\mathbf{p}\left({}^id^2 - 2R\left({}^i_ix\cos\theta_v + {}^i_iy\sin\theta_v\right)\right) \tag{34}$$

$$\|{}^i_i\boldsymbol{\ell}_v\| = \frac{1}{{}^id}\left({}^id^2 - 2R\left({}^i_ix\cos\theta_{N_v} + {}^i_iy\sin\theta_{N_v}\right)\right) \tag{35}$$

Substituting into Eq. (7) for $N_s = 1$ yields Eq. (13). Now, we only have to differentiate the expression for energy and set it to zero to obtain Eq. (14).

References

[1] D. Rus and M. T. Tolley, "Design, fabrication and control of soft robots," *Nature*, vol. 521, no. 7553, pp. 467–475, May 2015.

[2] L. Blanc, A. Delchambre, and P. Lambert, "Flexible medical devices: Review of controllable stiffness solutions," *Actuators*, vol. 6, no. 3, 2017.

[3] S. Kim, C. Laschi, and B. Trimmer, "Soft robotics: A bioinspired evolution in robotics," *Trends in Biotechnology*, vol. 31, no. 5, pp. 287–294, 2013.

[4] M. Troise, M. Gaidano, P. Palmieri, and S. Mauro, "Preliminary analysis of a lightweight and deployable soft robot for space applications," *Applied Sciences (Switzerland)*, vol. 11, no. 6, pp. 1–12, 2021.

[5] L. Jin, A. E. Forte, B. Deng, A. Rafsanjani, and K. Bertoldi, "Kirigami-inspired inflatables with programmable shapes," *Advanced Materials*, vol. 32, no. 33, p. 2001863, 2020.

[6] J. I. Lipton, R. MacCurdy, Z. Manchester, L. Chin, D. Cellucci, and D. Rus, "Handedness in shearing auxetics creates rigid and compliant structures," *Science*, vol. 360, no. 6389, pp. 632–635, 2018.

[7] M. Trumić, K. Jovanović, and A. Fagiolini, "Decoupled nonlinear adaptive control of position and stiffness for pneumatic soft robots," *International Journal of Robotics Research*, vol. 40, no. 1, pp. 277–295, 2021.

[8] J. Choi, D.-Y. Lee, J.-H. Eo, Y.-J. Park, and K.-J. Cho, "Tendon-driven jamming mechanism for configurable variable stiffness," *Soft Robotics*, vol. 8, no. 1, pp. 109–118, 2021.

[9] W. Chen, S. Misra, Y. Gao, Y. Lee, D. E. Koditschek, S. Yang, and C. R. Sung, "A programmably compliant origami mechanism for dynamically dexterous robots," *IEEE Robotics and Automation Letters*, vol. 5, no. 2, pp. 2131–2137, 2020.

[10] C. Anders, H. Wagner, C. Puta, R. Grassme, A. Petrovitch, and H.-C. Scholle, "Trunk muscle activation patterns during walking at different speeds," *Journal of Electromyography and Kinesiology*, vol. 17, no. 2, pp. 245–252, 2007.

[11] Z. Shen and J. Seipel, "Animals prefer leg stiffness values that may reduce the energetic cost of locomotion," *Journal of Theoretical Biology*, vol. 364, pp. 433–438, 2015.

[12] A. Bergmark, "Stability of the lumbar spine: a study in mechanical engineering," *Acta Orthopaedica Scandinavica*, vol. 60, no. sup230, pp. 1–54, 1989.

[13] W. Shan, T. Lu, and C. Majidi, "Soft-matter composites with electrically tunable elastic rigidity," *Smart Materials and Structures*, vol. 22, no. 8, p. 085005, 2013.

[14] H. Rodrigue, W. Wang, M.-W. Han, T. Kim, and S.-H. Ahn, "An overview of shape memory alloy-coupled actuators and robots," *Soft Robotics*, vol. 4, no. 1, pp. 3–15, 2017.

[15] Z. Xing, F. Wang, Y. Ji, D. McCoul, X. Wang, and J. Zhao, "A structure for fast stiffness-variation and omnidirectional-steering continuum manipulator," *IEEE Robotics and Automation Letters*, vol. 6, no. 2, pp. 755–762, 2021.

[16] P. Lloyd, A. K. Hoshiar, T. da Veiga, A. Attanasio, N. Marahrens, J. H. Chandler, and P. Valdastri, "A learnt approach for the design of magnetically actuated shape forming soft tentacle robots," *IEEE Robotics and Automation Letters*, vol. 5, no. 3, pp. 3937–3944, 2020.

[17] C. Majidi, "Soft robotics: A perspective—current trends and prospects for the future," *Soft Robotics*, vol. 1, no. 1, pp. 5–11, 2014.

[18] I. Robert J. Webster and B. A. Jones, "Design and kinematic modeling of constant curvature continuum robots: A review," *The International Journal of Robotics Research*, vol. 29, no. 13, pp. 1661–1683, 2010.

[19] T. George Thuruthel, Y. Ansari, E. Falotico, and C. Laschi, "Control strategies for soft robotic manipulators: A survey," *Soft Robotics*, vol. 5, no. 2, pp. 149–163, 2018.

[20] A. K. Mishra, A. Mondini, E. Del Dottore, A. Sadeghi, F. Tramacere, and B. Mazzolai, "Modular continuum manipulator: Analysis and characterization of its basic module," *Biomimetics*, vol. 3, no. 1, 2018.

[21] D. Trivedi, A. Lotfi, and C. D. Rahn, "Geometrically exact models for soft robotic manipulators," *IEEE Transactions on Robotics*, vol. 24, no. 4, pp. 773–780, 2008.

[22] L. L. Howell, *Compliant mechanisms*. New York, NY, USA: John Wiley & Sons, 2001.

[23] M. Koehler, A. M. Okamura, and C. Duriez, "Stiffness control of deformable robots using finite element modeling," *IEEE Robotics and Automation Letters*, vol. 4, no. 2, pp. 469–476, 2019.

[24] P. Rao, Q. Peyron, S. Lilge, and J. Burgner-Kahrs, "How to model tendon-driven continuum robots and benchmark modelling performance," *Frontiers in Robotics and AI*, vol. 7, p. 223, 2021.

[25] A. Doroudchi, S. Shivakumar, R. E. Fisher, H. Marvi, D. Aukes, X. He, S. Berman, and M. M. Peet, "Decentralized control of distributed actuation in a segmented soft robot arm," in *2018 IEEE Conference on Decision and Control (CDC)*, 2018, pp. 7002–7009.

[26] P. Polygerinos, S. Lyne, Z. Wang, L. F. Nicolini, B. Mosadegh, G. M. Whitesides, and C. J. Walsh, "Towards a soft pneumatic glove for hand rehabilitation," in *IEEE/RSJ International Conference on Intelligent Robots and Systems*, 2013, pp. 1512–1517.

[27] S. Huang, D. Meng, X. Wang, B. Liang, and W. Lu, "A 3D static modeling method and experimental verification of continuum robots based on pseudo-rigid body theory," in *IEEE/RSJ International Conference on Intelligent Robots and Systems (IROS)*, 2019, pp. 4672–4677.

[28] J. Carlson, J. Friedman, C. Kim, and C. Sung, "REBOund: Untethered origami jumping robot with controllable jump height," in *IEEE International Conference on Robotics and Automation (ICRA)*, 2020, pp. 10 089–10 095.

[29] Y. Kim, S. S. Cheng, and J. P. Desai, "Active stiffness tuning of a spring-based continuum robot for MRI-guided neurosurgery," *IEEE Transactions on Robotics*, vol. 34, no. 1, pp. 18–28, 2018.

[30] D. Zappetti, R. Arandes, E. Ajanic, and D. Floreano, "Variable-stiffness tensegrity spine," *Smart Materials and Structures*, vol. 29, 2020.

[31] Y. Yuan and C. Sung, "Programmable stiffness and applications of 3D printed TPU diamond lattices," in *ASME/International Design Engineering Technical Conferences and Computers and Information in Engineering Conference*, 2021.